ACS NANO

www.acsnano.org

ARTICLE

An Ultralocalized Cas13a Assay Enables Universal and Nucleic Acid Amplification-Free Single-Molecule RNA Diagnostics

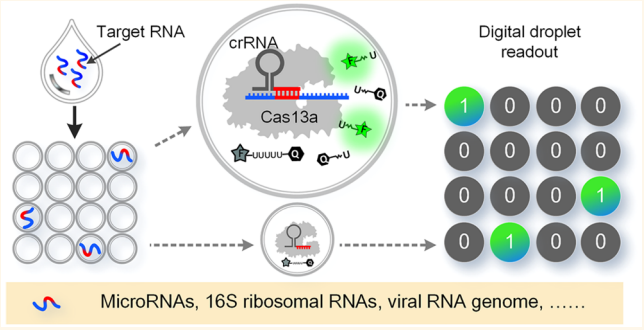
Tian Tian, Bowen Shu,* Yongzhong Jiang, Miaomiao Ye, Lei Liu, Zhonghui Guo, Zeping Han, Zhang Wang, and Xiaoming Zhou*

Cite This: https://dx.doi.org/10.1021/acsnano.0c08165

Read Online

ACCESS | Metrics & More | Article Recommendations | Supporting Information

ABSTRACT: Existing methods for RNA diagnostics, such as reverse transcription PCR (RT-PCR), mainly rely on nucleic acid amplification (NAA) and RT processes, which are known to introduce substantial issues, including amplification bias, cross-contamination, and sample loss. To address these problems, we introduce a confinement effect-inspired Cas13a assay for single-molecule RNA diagnostics, eliminating the need for NAA and RT. This assay involves confining the RNA-triggered Cas13a catalysis system in cell-like-sized reactors to enhance local concentrations of target and reporter simultaneously, *via* droplet microfluidics. It achieves >10 000-fold enhancement in sensitivity when compared to the bulk Cas13a assay and enables absolute digital single-molecule RNA quantitation. We experimentally demonstrate its broad applicability for precisely counting microRNAs, 16S rRNAs, and SARS-CoV-2 RNA from synthetic sequences to clinical samples with excellent accuracy. Notably, this direct RNA diagnostic technology enables detecting a wide range of RNA molecules at the single-molecule level. Moreover, its simplicity, universality, and excellent quantification capability might render it to be a dominant rival to RT-qPCR.



KEYWORDS: *RNA diagnostics, CRISPR-Cas13a, droplet microfluidics, liquid biopsy, SARS-CoV-2*

Due to the essential roles in numerous biological processes, RNA molecules served as the detection targets with great value in diverse areas, ranging from biomedical research to clinical diagnostics. Technological advancements over the past decades have brought forth various RNA detection technologies, which can be categorized into direct or nucleic acid amplification (NAA)-based detection. The classical methods for direct RNA detection, such as Northern blotting,[1] FISH,[2] and microarrays,[3,4] are advantageous in terms of high fidelity, but they are often labor-intensive and time-consuming and suffer from poor sensitivity. Such situations have been ameliorated, to some extent, by the recently developed strategies for direct RNA detection.[5−14] However, the limitations with respect to limited sensitivity,[10,14] complex procedures,[12,13] or requiring exclusive instruments and resources[6,8−13] hamper their wide application. While most of these methods prove their success for short RNA sequence detection, such as microRNA,[6,8−13] the applicability for detecting long-chain RNA with more complex structures (such as mRNA, rRNA, or viral RNA) is rarely investigated. NAA-based RNA detection techniques, including reverse transcription PCR (RT-PCR)[15,16] and other isothermal amplification methods,[17] are routinely used for highly sensitive RNA detection, but they generally require the conversion of RNA to DNA and subsequent template replication steps. These steps often introduce substantial issues including sample loss resulting from the incomplete RT step, amplification bias caused by error-prone sequence replication, and false-positive risk due to contamination. These issues could be disastrous when ultrasensitive and quantitative detection of RNA molecules is of particular need for routine diagnosis of infectious disease, such as the quantification of viral load for human immunodeficiency virus and the genetic identification of SARS-CoV-2-causing infection during the COVID-19

Received: September 28, 2020
Accepted: December 14, 2020

Downloaded via UNIV OF GOTHENBURG on December 19, 2020 at 03:36:04 (UTC).
See https://pubs.acs.org/sharingguidelines for options on how to legitimately share published articles.

© XXXX American Chemical Society

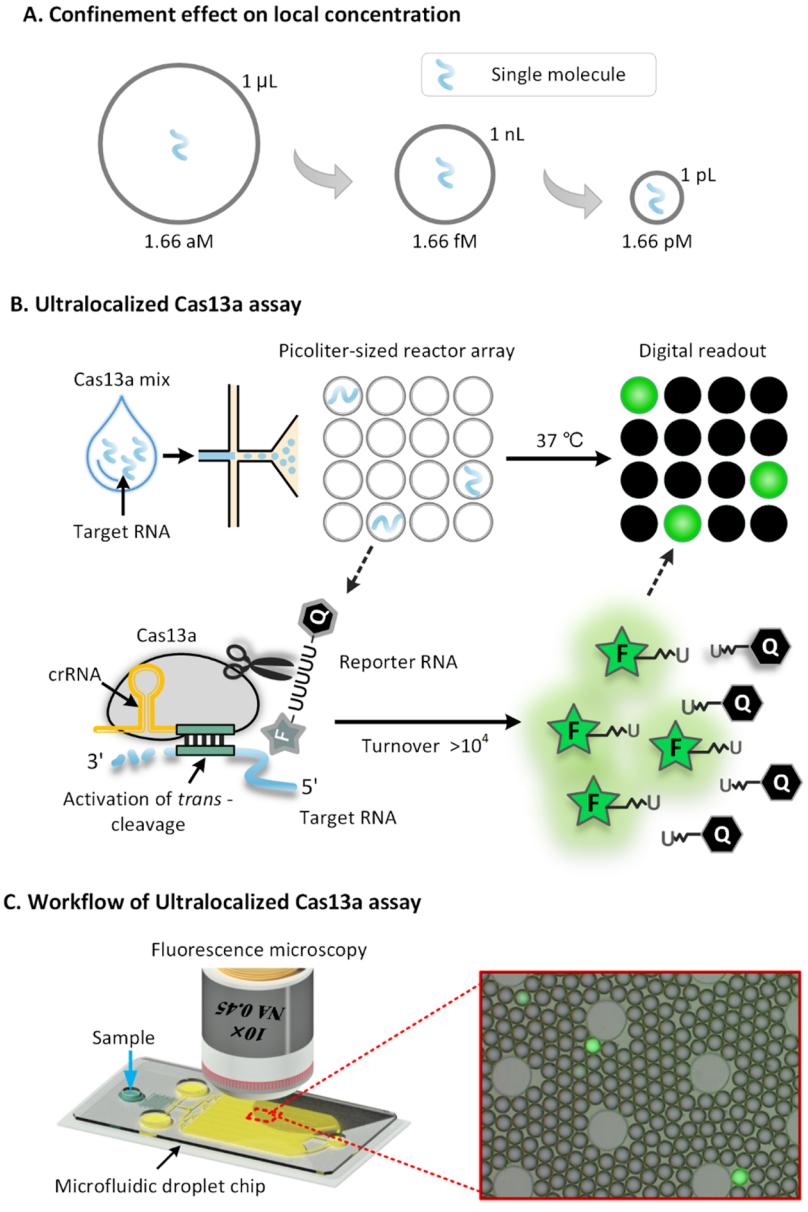


Figure 1. Concept of ultralocalized Cas13a assay. (A) Confinement effect on local concentration. The local concentration of a single molecule increases inversely with decreasing analytical volume. (B) Schematic of the ultralocalized Cas13a assay. Target RNAs (light blue) together with a Cas13a mixture are emulsified with oil into thousands of picoliter-sized droplet reactors. After recognition by a crRNA (yellow), single-target RNA will induce cleavage of over 10^4 quenched fluorescent RNA reporters (F, fluorescence; Q, quencher), thus yielding a fluorescently positive droplet. (C) Workflow of the ultralocalized Cas13a assay. By coupling a microfluidic droplet chip with fluorescence microscopy, highly uniform microdroplets are robustly generated and self-assembled into a monolayer droplet array for fluorescence imaging-based droplet counting.

pandemic. Therefore, it is essential to develop universal detection methods for RNA diagnostics that not only obtain PCR-like sensitivity but also avoid NAA-related issues.

The recently discovered clustered regularly interspaced short palindromic repeats (CRISPR) effector Cas13a in prokaryotes has provided further opportunities for RNA detection.[18,19] As an RNA-guided RNA-targeting effector, Cas13a possesses the target-dependent *trans*-cleavage mechanism linking highly specific target recognition and highly processive cleavage of nearby reporter molecules, which allows developing advanced sensing strategies for direct RNA detection without reverse transcription. However, the direct Cas13a assay could only detect RNA at sub-pM concentrations.[20−22] The insufficient sensitivity will hinder its applications in which detecting RNA target at the aM level is a critical need, such as liquid biopsy and pathogen detection from clinical samples. Recently, a more sensitive Cas13a-based technique termed SHERLOCK has been explored for RNA detection, exhibiting single-molecule sensitivity and single-nucleotide specificity.[23−26] But this technique still retains the weaknesses of NAA-based methods, because of the introduction of RT, T7 RNA polymerase transcription and recombinase polymerase amplification.

Herein, we attempted to circumvent these issues by learning from the natural confinement effect. It is well known that the various interaction-based biochemical reactions occurring within the cell are very efficient, although the amount of substrate molecules for these reactions was very minimal.[27,28] For instance, most mRNAs' expression level is lower than 100

https://dx.doi.org/10.1021/acsnano.0c08165
ACS Nano XXXX, XXX, XXX−XXX

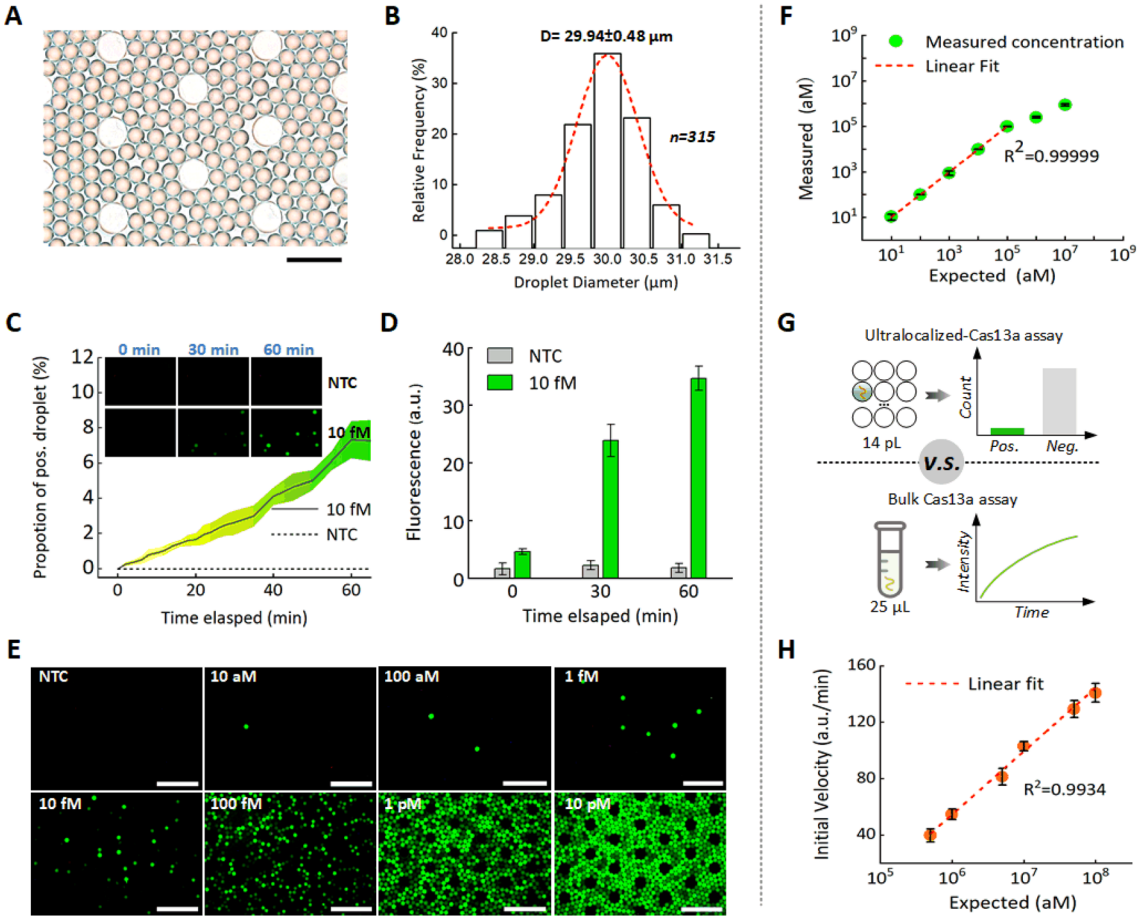


Figure 2. Quantitation performance of the ultralocalized Cas13a assay. (A) Microscopic photography of picoliter-sized droplets under a 10× objective lens (scale bar: 100 μm). (B) Size distribution of the droplets. (C) Time course of the proportion of positive droplet (PPD) for single-molecule miRNA detection that underwent a 37 °C incubation. (D) Background-subtracted fluorescence difference between the positive and negative droplets during single-molecule miRNA detection *via* the ultralocalized Cas13a assay. (E) Representative end-point fluorescence images of various miRNA-17 concentrations for the ultralocalized Cas13a assay (10× magnification, scale bar: 200 μm). (F) Quantification range of the ultralocalized Cas13a assay. (G) Schematic concept of the ultralocalized Cas13a assay and bulk Cas13a assay. (H) Quantitation range of synthetic miRNA-17 using the bulk Cas13a assay, in which the initial velocity is defined as $\Delta F/\Delta T$. Here, ΔF represents the change of the fluorescence intensity before reaching a plateau, and ΔT is the corresponding time frame. All experiments shown above are repeated three times, and bars represent mean ± s.e.m.

copies per cell.[29] It is quite difficult to detect such a minimal number of mRNA molecules *in vitro* (*e.g.*, in a PCR tube) without the aid of NAA. However, it is easy to visualize these mRNA molecules in a cell using fluorescent probe-based imaging techniques.[30] A key factor of this phenomenon is the confinement effect, which promotes the local molecule concentration for highly efficient reaction or detection. We wondered whether an *in vitro* Cas13a assay confined in a cell-sized volume could reproduce a similar outcome to enable detection of less than 100 copies of RNA per cell. To verify this concept, we performed the Cas13a assay in picoliter-sized droplets by droplet microfluidics. We found that the accumulated fluorescent signal from a single RNA target-activated Cas13a's collateral cleavage is sufficient to illuminate a picoliter-sized droplet, thus enabling NAA-free and digital RNA quantification at the single-molecule level. Moreover, we explored its applicability for precise counting of cell-free microRNAs from clinical serum samples, ultrasensitive detection of 16S rRNA from uropathogens, and accurate diagnosis of SARS-CoV-2 with 100% concordance with RT-qPCR results.

RESULTS AND DISCUSSION

Concept and Construction of an Ultralocalized Cas13a Assay. Different from the strategies based on amplifying the target itself or the detection signal, herein we harness a bioinspired confinement effect for sensitivity enhancement. As illustrated in Figure 1A, the presence of a single molecule in a bulk volume, such as one microliter, yields an aM level molecular concentration that is beyond the detection limit of the most conventional biochemical assays or detectors. If the single molecule is confined in a volume of 1 nL or 1 pL, its local concentration will increase to 1.66 fM or 1.66 pM, respectively. When the molecule acts as a trigger of biochemical reaction, the enhanced molecular concentration is known to promote the reaction efficiency; when it severs as a signal reporter, the yielded high local concentration is detected by an ordinary detector. Coincidentally, the Cas13a assay is a homogeneous method that relies on the target RNA recognition triggered *trans*-cleavage of quenched fluorescent reporters.[31−33] The bienhancement of the local concentration of target and reporter *via* ultralocalization could potentially

https://dx.doi.org/10.1021/acsnano.0c08165
ACS Nano XXXX, XXX, XXX−XXX

promote this assay to be an ultrasensitive RNA detection technology, which we termed as ultralocalized Cas13a assay.

This concept can be verified by performing the Cas13a assay in picoliter-scale reactors *via* droplet microfluidics. As schematically illustrated in Figure 1B, a mix of the target RNA molecules, Cas13a, crRNAs, and fluorescently labeled RNA reporters are compartmentalized into several tens of thousands of monodisperse picoliter-sized droplets and subsequently assembled to a high-density droplet array for *in situ* incubation and fluorescence imaging. During the incubation, the target RNA can be specifically recognized by the programmable crRNA of the Cas13a system. On binding a target RNA sequence, Cas13a becomes activated and continuously cleaves the self-quenched fluorescent RNA reporters with an extraordinarily high turnover ($>10^4$).[22] The high-yielding fluorescent signal confined in an ultrasmall volume could be facilely accumulated to illuminate a droplet. Meanwhile, in the absence of the RNA target, Cas13a activation, cleavage of the reporter RNAs, and generation of fluorescence do not occur. If a single RNA target molecule is sufficient to "light up" a droplet in this way, digital counting of single RNA molecules can be achieved by assigning each positive and negative droplet as "one" and "zero". As such, the RT-free, NAA-free, and absolute RNA quantification can be realized.

Noting that the Cas13a assay is an isothermal and one-step reaction, the entire workflow can be implemented using a syringe-vacuum-driven microfluidic droplet chip coupled with a standard fluorescence microscopy (Figure 1C). Once pipetting the Cas13a mixture on the sample inlet, highly uniform microdroplets can be robustly generated and subsequently self-assembled into a droplet array by withdrawing the piston of a connecting syringe. The resulting droplet array can be *in situ* detected by fluorescence imaging-based droplet counting, without the need for droplet transfer.

Single-Molecule MicroRNA Detection and Quantification. To mimic the confinement effect of a cell, we constructed a microfluidic droplet platform to conduct the ultralocalized Cas13a assay in cell-like-size droplets (Supplementary Figure S1). This platform is capable of high-throughput generation of monodisperse picoliter-sized droplets with minimal sample consumption (Figure 2A and Supplementary Video S1). The generated droplets are highly uniform (approximately 30 μm in diameter with CV < 1.7%) and have a similar diameter to a human mammalian cell (Figure 2B). Moreover, up to 10^5 droplets can be generated on the microfluidic chip within 3 min. These features facilitate investigating the confinement effect on the Cas13a assay in highly paralleled and identical conditions.

To evaluate this effect on the Cas13a assay, we used 10 fM ($\sim 6 \times 10^3$ copies per μL) synthetic miRNA-17 as input. At this target concentration, each droplet contains no more than one target molecule with a probability of 99.67%, which means there is almost single-target RNA included in a "target-containing" droplet. We observed the time course of the proportion of fluorescence positive droplet (PPD) during *in situ* isothermal incubation (37 °C). The PPD of the single-molecule assay approached a plateau around 60 min, and no positive droplet was found in no-template-control (NTC) experiments (Figure 2C).

Further, the statistical data show that 10 fM synthetic miRNA-17 yielded a robust measured value that agreed closely with the predicted value (8.4%) (Figure 2C). Even if it takes up to 15 min to initialize droplet generation, the premature Cas13a's *trans*-activity in the Cas13a mix could hardly cause overestimation of RNA abundance (Supplementary Figure S2). The *trans*-cleavage activity of Cas13a triggered by the binding of the target RNA could subsequently cleave collateral RNA reporters in a nonspecific manner.[32] Once the activated Cas13a is encapsulated into a droplet, its continuous *trans*-cleavage of the self-quenched fluorescent RNA reporters is confined in this droplet. Although some RNA reporters are also cleaved by this activated Cas13a prior to droplet formation, these reporters were highly diluted when they subsequently dispersed into several tens of thousands of droplets. The highly diluted reporters could hardly generate enough fluorescence signal comparable to those of the true positive droplets containing either RNA target or activated Cas13a. This is different from the NAA-based droplet digital assay; the preamplified sequences prior to droplet formation could also serve as templates to generate indistinguishable positive events. This evidence reveals that the ultralocalized Cas13a assay is capable of single-molecule miRNA detection, which merely requires a 60 min isothermal incubation. The low temperature for Cas13a mix preparation (below 25 °C), combined with a short time frame (<3 min) for droplet generation, could minimize the premature Cas13a's *trans*-activity (Supplementary Figure S3). Consequently, an evident difference (~20-fold) in the fluorescence signal between the positive and negative reactors could be measured (Figure 2D and Supplementary Figure S4), which is favorable for accurate binarization of the resulting reactors in the subsequent digital assay.

To investigate the quantification capability, we tested the ultralocalized Cas13a assay using serial dilutions of known concentrations of synthetic miRNA-17 (10^1 to 10^7 aM). The end-point fluorescence images displayed an apparent consistency between the input concentration and PPD (Figure 2E). An excellent ($R^2 > 0.9999$) linear response was also observed between the measured concentration and the input concentration in the dynamic range from 10^1 to 10^5 aM (Figure 2F). Although target concentrations over 10^5 aM were also quantified, an underestimation of the input concentration occurred despite using Poisson distribution correction. Noting that the bulk-volume Cas13a assay using the same cocktail could only obtain a limit of detection of 500 fM (Figure 2G,H and Supplementary Figure S5), over 10^4-fold enhancement in sensitivity was achieved by the ultralocalized Cas13a assay. Further, the current amplification-free assay has an extended lower limit of quantification compared with the well-established RT-qPCR assay, in which as low as 100 aM miRNA could be quantified (Supplementary Figure.S6).

Quantitative Analysis of miRNA in Complex Matrices. Prior to analyzing miRNA in complex matrices, we examined the analytical specificity of the ultralocalized Cas13a assay. Here, we first discriminated miRNAs from different families including miRNA-17, -10b, -21, and -155 using truncated miRNA-17 targeted crRNAs with a 20-nt spacer (Supplementary Figure S7). The miRNA-17 complementary to the crRNA yielded over a 200-fold increase in outcomes compared to those obtained with the other three miRNAs when using an equal amount of input. To investigate its selectivity, we tested the ultralocalized Cas13a assay with mixtures of these miRNAs at 1:1 molar ratio. As expected, the outcome of miRNA-17 including a mixture ("Mix 4") showed no significance to that of the individual miRNA-17 assay, and the miRNA-17-excluded

https://dx.doi.org/10.1021/acsnano.0c08165
ACS Nano XXXX, XXX, XXX−XXX

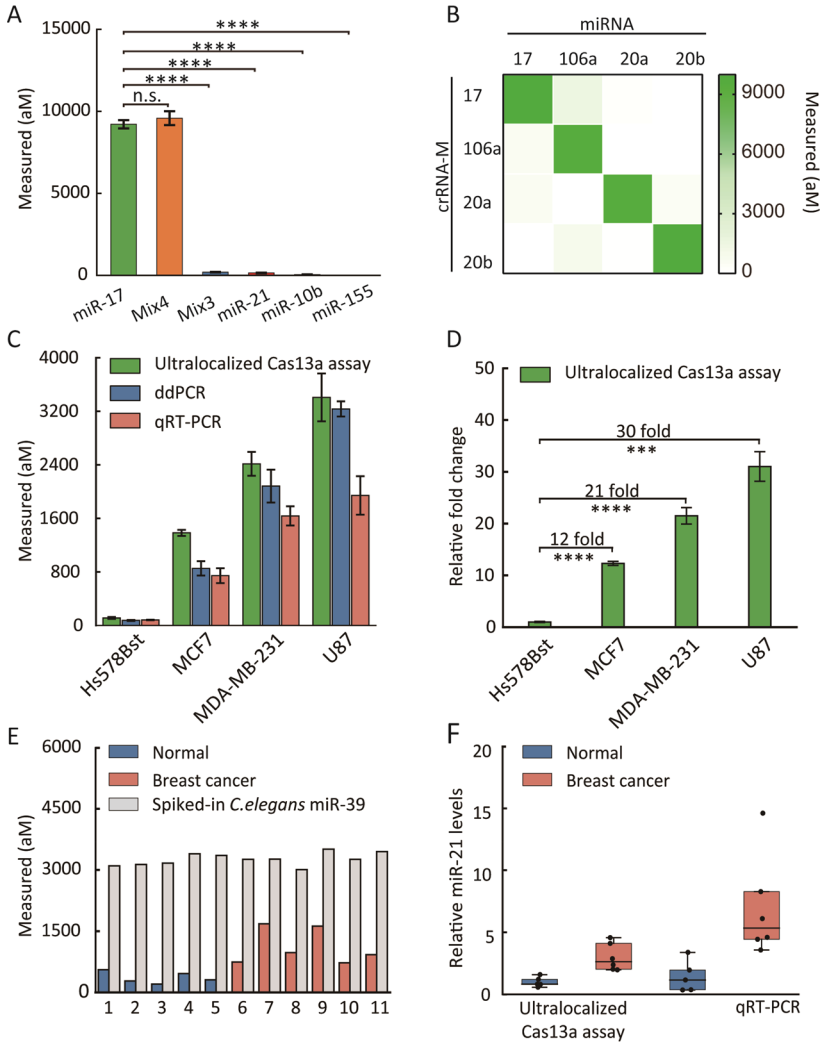


Figure 3. Direct miRNA analysis in synthetic sequences and cancer-derived serum samples using the ultralocalized Cas13a assay. (A) Detection of four miRNAs from different families utilizing crRNA complementary to miRNA-17. Mix 4 represents the mixture of four miRNAs (miRNA-17, -21, -10b, and -155), and Mix 3 represents the Mix 4 mixture excluding miRNA-17. The final concentration of each miRNA in these assays was 10 fM (two-tailed Student's *t* test; ****, $p < 0.0001$). (B) Heat map analysis of the orthogonal identification of four homologous miRNAs. (C) Evaluation of miRNA-17 expression in the total small RNA extracts (10 pg per μL) using qRT-PCR, ddPCR, and ultralocalized-Cas13a assay. (D) miRNA-17 relative expression levels in the total small RNA extracts (10 pg per μL) measured by the ultralocalized Cas13a assay (from C) (two-tailed Student's *t* test; ***, $p < 0.001$; ****, $p < 0.0001$). (E) Absolute quantification of miRNA-21 in serum derived from six breast cancer patients and five healthy donors using the ultralocalized Cas13a assay. MiRNA-39 spiked-in control was used to normalize the efficiency of extraction. (F) Box and whisker plots of miRNA-21 relative expression by the ultralocalized-Cas13a assay and qRT-PCR. Boxes mark the intervals between the 25th and 75th percentiles. Black lines inside the boxes represent medians. Whiskers indicate the intervals between the 5th and 95th percentiles. Black dots denote data points outside the 5th and 95th percentiles. All the experiments shown above were replicated three times, and bars represent mean ± s.e.m.

mixture ("Mix 3") gave a similar outcome to that of the individual assay of the other three miRNAs (Figure 3A). To further demonstrate the specificity, we challenged the ultralocalized Cas13a assay with highly homologous miRNAs (-17, -106a, -20a, and -20b), which belong to the same family and differ by just one or two nucleotides. Considering that the Cas13a system has a tolerance for one mismatch but is sensitive to two or more mismatches in the crRNA spacer:target duplex,[20,23] herein we introduced an artificial mismatch in the crRNA spacer sequences (Supplementary Figures S7 and S8). The orthogonal testing result displayed the successful discrimination and ultralow cross-reactivity, indicating the ultralocalized Cas13a assay has excellent specificity for discriminating homologous sequences, even those with single-nucleotide differences (Figure 3B).

To assess the utility for accurate quantification in complex samples, we used the ultralocalized Cas13a assay to quantify miRNA-17 expression levels in four different cell lines, including human breast normal cells (Hs578Bst), adenocarcinoma cells (MCF-7 and MDA-MB-231), and human glioma cells (U87). Overall, the relative expression levels of miRNA-17 in different cell lines using the ultralocalized Cas13a assay show similar variations to those measured with qRT-PCR and ddPCR and reveal significant differences in miRNA-17 expression between the normal cell lines and the cancer-related cell lines (Figure 3C and D). Compared with the results from qRT-PCR and ddPCR, a slightly higher level of miRNA-17 expression was measured in each cell line using the ultralocalized Cas13a assay. This might be attributed to the

https://dx.doi.org/10.1021/acsnano.0c08165
ACS Nano XXXX, XXX, XXX−XXX

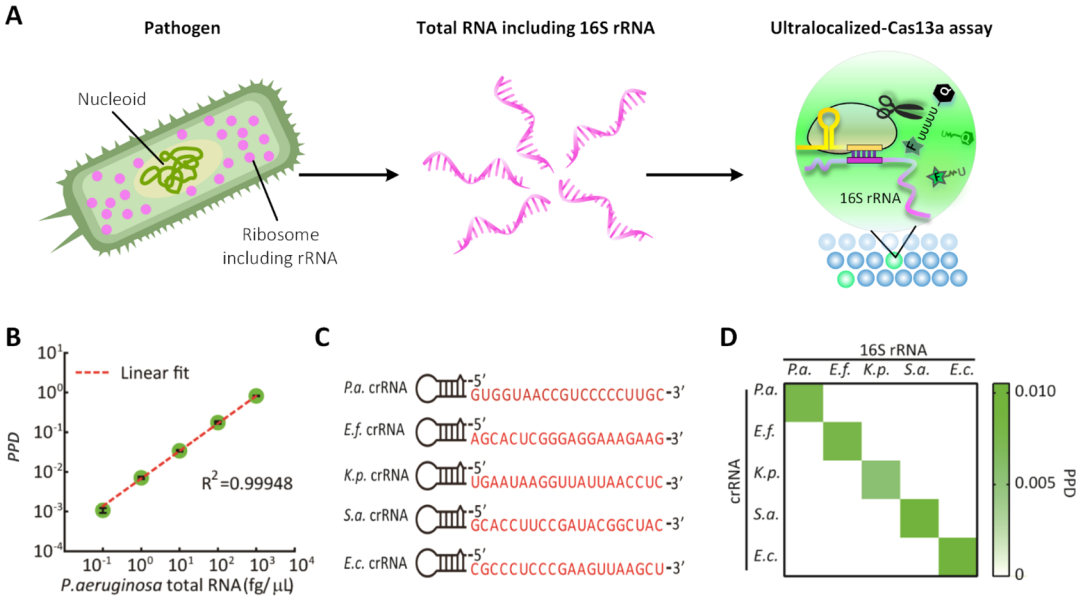


Figure 4. 16S rRNA-targeted ultralocalized Cas13a assay for pathogen detection. (A) Schematic of 16S rRNA-targeted pathogen detection using the ultralocalized Cas13a assay. Total RNA is extracted from bacterial cells, and target regions within the 16S rRNA are recognized by the designed crRNA to trigger the ultralocalized *trans*-cleavage of quenched fluorescent reporters, with the resulting droplets producing detectable fluorescence signals to indicate the presence and amount of the target of interest. (B) Detection of *P.a.* 16S rRNA in total RNA sample using the ultralocalized Cas13a assay. Concentrations of total RNA for the ensemble readout ranged from 0.1 fg to 1 pg per μL. (C) Species-specific crRNAs for identification a panel of uropathogens, including *Pseudomonas aeruginosa* (*P.a.*), *Enterococcus faecalis* (*E.f.*), *Klebsiella pneumoniae* (*K.p.*), *Staphylococcus aureus* (*S.a.*), and *Escherichia coli* (*E.c.*). The red letters represent the spacer region. (D) Heatmap analysis of the orthogonal identification of five uropathogens. The total RNA used for analysis is 1 fg/μL for five uropathogens, respectively.

high fidelity of amplification-free quantification, which avoids amplification bias and sample loss during reverse transcription.

This capability encourages us to apply the ultralocalized Cas13a assay for distinguishing the serum miRNA-21 levels from breast cancer patients and healthy individuals. In this experiment, 11 serum specimens from six breast cancer patients and five healthy donors were tested, and the miRNA-39 spiked-in controls were used to indicate the deviations among the individual RNA extracts (Figure 3E). Collectively, the quantitative results from the ultralocalized Cas13a assay reveal a 2.9-fold up-regulation of the miRNA-21 level in breast cancer patients' serum, which is consistent with those reported previously.[34] The results were further confirmed by the well-established qRT-PCR method, which gave an average of 4.8-fold up-regulation with greater variability (Figure 3F and Supplementary Figure S9).

Ultrasensitive Detection of Uropathogen 16S rRNAs. Motivated by the success in detecting the short-sized miRNA, we wonder whether the ultralocalized Cas13a assay could also be applicable for large-sized RNA detection. To verify this, we chose bacterial 16S rRNA (16S rRNA), a structure RNA with a sequence size approaching 1500 nucleotides, as a proof-of-concept model. As an initial attempt, we tested the Cas13a assay through direct targeting of the sequence of 16S rRNAs (Figure 4A). Here, a crRNA to specifically target 16S rRNA of *Pseudomonas aeruginosa* (*P.a.*) was designed, and the targeted 16S rRNA sequences together with other total RNAs extracted from *P.a.* cells were tested. The bulk-volume Cas13a assay showed that the designed crRNA has excellent selectivity (Supplementary Figure S10). However, the bulk detection could only detect this 16S rRNA in total RNA at subng levels (Supplementary Figure S11). We anticipated a more sensitive 16S rRNA detection could be achieved by the ultralocalized Cas13a assay. To validate this, we used serially diluted total RNA extracts from *P.a.* as input. We found that it was able to detect 16S rRNAs in a 0.1 fg/μL total RNA sample and linearly respond to input concentrations from 0.1 fg/μL to 1 pg/μL (Figure 4B). This sensitivity for detection of *P.a.* total RNA represents a calculated quantity of approximately 6 cells per 10 mL, assuming a total RNA amount of 170 fg per *P.a.* cell.[35] Given the natural high abundance of 16S rRNAs in a bacterial cell (over 10^4 copies per cell),[36] the sensitivity obtained here is also approximately equivalent to 6 copies of 16S rRNAs per μL. This means this amplification-free Cas13a assay could determine the presence of a single viable pathogen in a 1 mL volume.

To check its specificity for species-specific identification, we designed a set of organism-specific crRNAs to distinguish five common pathogens responsible for urinary tract infections (UTIs): *Pseudomonas aeruginosa* (*P.a.*), *Enterococcus faecalis* (*E.f.*), *Klebsiella pneumoniae* (*K.p.*), *Staphylococcus aureus* (*S.a.*), and *Escherichia coli* (*E.c.*) (Figure 4C). As expected, the orthogonal testing confirmed this assay was able to discriminate these five pathogens with desired levels of specificity (Figure 4D).

Molecular Diagnosis of SARS-CoV-2 Infection from Clinical Samples. Having shown successful quantification of 16S rRNAs, we reconfigured our platform to exploit the potential for detecting large-sized complex RNA molecules, such as RNA virus genome. Here, SARS-CoV-2 RNA with a sequence size approaching 30 000 nucleotides was selected as a target to develop the ultralocalized Cas13a assay (Figure 5A). The corresponding crRNAs were designed to target the open reading frame 1a (O) gene and nucleocapsid (N) gene of the SARS-CoV-2 viral genome (Figure 5B) and were optimized to avoid structured self-hybridization in the spacer region

https://dx.doi.org/10.1021/acsnano.0c08165
ACS Nano XXXX, XXX, XXX−XXX

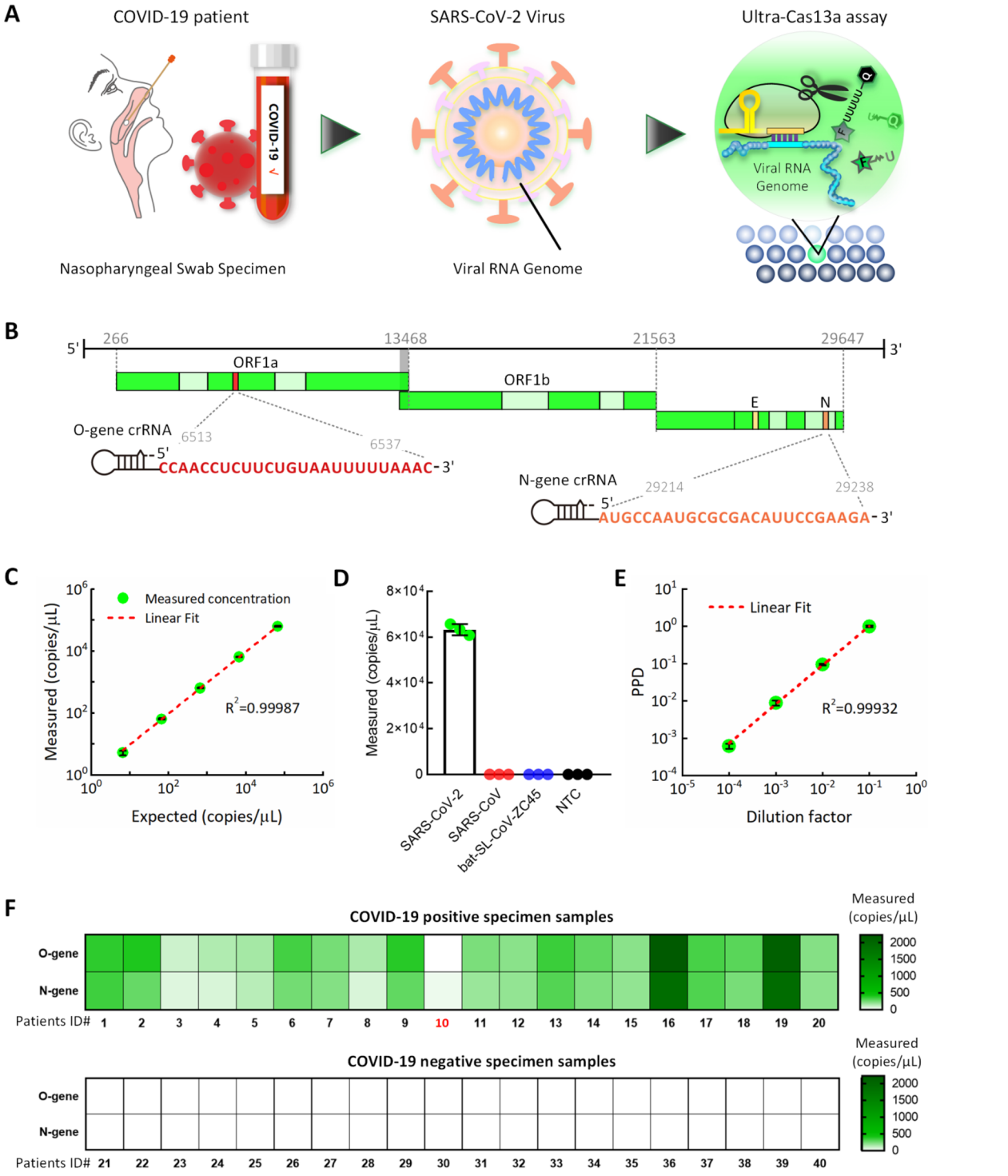


Figure 5. Ultralocalized Cas13a assay for detection of SARS-CoV-2. (A) Schematic of clinical diagnosis of SARS-CoV-2 using the ultralocalized Cas13a assay. Total RNAs are extracted from clinical nasopharyngral swab samples. When target regions within a viral RNA genome was recognized by the designed crRNAs in a droplet, they will trigger the *trans*-cleavage of quenched fluorescent reporters, thus "lighting up" the droplet to indicate the presence of the target of interest. (B) SARS-CoV-2 genome map showing Orf1a (O) and nucleocapsid (N) gene regions chosen for the ultralocalized Cas13a assay. (C) Assessment of the quantification ability of the ultralocalized Cas13a assay by detecting the N-gene, using serially diluted *in vitro* synthesized SARS-CoV-2 RNA standards. (D) Assessment of the specificity of the ultralocalized Cas13a assay. N-gene crRNA was designed to specifically target SARS-CoV-2. (E) Quantitation of the full-length SARS-Cov-2 RNAs by targeting the N-gene. The correlation between the dilution factor and PPD is $Y = 9.6552*X - 3.5025 \times 10^{-4}$ (R^2 = 0.999 32). (F) Ultralocalized Cas13a assay-enabled quantitative diagnosis of SARS-CoV-2 infection. Here, 40 clinical nasopharyngeal swab specimens collected from suspected COVID-19 patients were tested.

(Supplementary Figure S12). We first evaluated the effectiveness of this assay using serially diluted SARS-CoV-2RNA standards with N-gene crRNA and observed a reproducible detection limit down to ~6 copies/μL and an excellent

https://dx.doi.org/10.1021/acsnano.0c08165
ACS Nano XXXX, XXX, XXX−XXX

linearity (R^2 = 0.99987) over 4 orders of magnitude (Figure 5C). Moreover, we investigated that this assay could specifically detect the N gene of SARS-CoV-2 with no cross-reactivity toward the related N gene sequences from other SARS-like coronavirus, including SARS-CoV and bat SARS-like coronavirus (Figure 5D). To test its efficiency in detecting full-length SARS-CoV-2 RNA, we applied this assay to quantify 10-fold dilutions of total RNA extracted from cultured SARS-CoV-2 ranging from 1:1 to 1:10^5 (Figure 5E). The excellent linear correlation between the dilution factor and PPD (R^2 = 0.999 32) reveals that this assay could accurately quantify the full-length viral RNA as expected.

We performed the ultralocalized Cas13a assay to analyze 40 clinical nasopharyngeal swab RNA extracts. These swab specimens were collected from suspected COVID-19 patients in Wuhan, China (during March 2020), and the RNA extracts of each specimen were immediately validated by the current gold standard for SARS-CoV-2 diagnosis: RT-qPCR. By targeting both the O-gene and N-gene, this assay correctly identified all COVID-19 positive and negative samples, with 100% concordance with RT-qPCR results (Figure 5F). Of these, we found sample #10 (highlighted in red) was identified as COVID-19 positive by N-gene-targeted ultralocalized Cas13a assay, but the O-gene in this sample was missed in the test. Moreover, the measured concentration of the N-gene in sample #10 was low (31 copies/μL). This result lead us to wonder the actual concentration and integrity of these clinical RNA samples used in the ultralocalized Cas13a assay, which have been stored for more than three months and undergone freeze−thaw and long-distance transportation. Thus, we immediately checked these RNAs by using the same diagnostic kit that was used for the first validation. The repeated RT-qPCR results show that both the O-gene and N-gene in all positive samples except sample #10 have threshold cycle numbers (Ct) ranging from 20.8 to 34.5, and the two genes were undetectable in all COVID-19-negative samples (Supplementary Figures S13 and S14). For sample #10, RT-qPCR gave a Ct value of 40.3 for the O-gene and 36.7 for the N-gene. Given that a Ct value beyond 38 is judged as negative according to the declaration of the diagnostic kit, the Ct values of sample #10 suggested that the N-gene copy number was indeed low and the O-gene was probably degraded. Noting that similar cases frequently occur in the clinical diagnosis of COVID-19,[37] a single gene-targeted diagnostic assay might not be reliable for genetic identification of SARS-CoV-2 infection due to partial RNA degradation. In this regard, it is advantageous to obviate false-negative results for this assay by the addition of crRNAs to cover additional loci among the SARS-CoV-2 viral genome.

Advantages, Limitation, and Outlook of the Ultralocalized Cas13a Assay. The discovery of the CRISPR-Cas system has revolutionized the field of biomedical research and clinical diagnostics.[38,39] Among the developed CRISPR-based diagnostic systems, the Cas13a system has more efficient *trans*-cleavage (turnover 10^4:1) and less stringent PAM site dependence.[33] The high efficiency allows the Cas13a assay to directly detect sub-pM RNA molecules in a bulk volume, taking advantage of a simple procedure (*e.g.*, fluorescent assay[20,31]) or simple readout (*e.g.*, electrochemical assay[40]). While single-molecule sensitivity can be obtained *via* the combination of T7 RNA polymerase transcription, NAA with the Cas13 system, such as SHERLOCK,[23,24,26,41] the multistep process is at risk of introducing amplification bias, sample loss, and cross-contamination.

Herein we proposed an ultralocalized Cas13a assay as an attractive alternative to achieve single-molecule sensitivity and eliminate NAA-related problems. A key element of this concept is harnessing the natural confinement effect to enhance the local concentration of target and reporter for the Cas13a system in ultraconfined volumes (*i.e.*, a cell-like size). We deduced that the dramatically increased molecular concentration (over 10^5-fold), incorporated with the high efficiency and specificity of the Cas13a system, could lead to an innovative RNA detection with PCR-like sensitivity in a simple fashion. We verified this concept by performing the Cas13a assay in picoliter-sized droplets, using a simple droplet microfluidic platform, and we found that the accumulated fluorescent signal from a single microRNA target-activated Cas13a's collateral cleavage is sufficient to illuminate a picoliter-sized droplet. This feature endows this assay with two important capabilities that the current Cas13a-based methods have not provided: NAA-free single-molecule detection and absolute digital quantification (Supplementary Note 1). Moreover, this success in the Cas13a system may introduce a route toward simple and highly sensitive nucleic acid detection for other CRISPR-Cas systems (*i.e.*, Cas12 and Cas14 families), owing to their available *trans*-cleavage mechanism.

Notably, compared to other state-of-the-art RNA detection technologies (Supplementary Note 2), the ultralocalized Cas13a assay is advantageous in term of simplicity and high sensitivity. For example, this presented method is a homogeneous assay, thus obviating the time-consuming washing steps required in those heterogeneous assays (*i.e.*, Simoa[12] and electrochemical methods[13]). With respect to the sensitivity, this method achieved single-molecule analytical sensitivity, which is 10^4-fold more sensitive than those reported methods, such as single-molecule fluorescence cross-correlation spectroscopy,[8] nanopore,[10] SiMREPS,[11] and miracles.[14] Furthermore, this method could achieve a 4 orders of magnitude dynamic range that covers the natural dynamic range of miRNA expression.[42] More importantly, we experimentally validated its broad applicability for quantifying diverse RNA molecules (such as miRNAs, bacterial 16S rRNAs, and viral genome RNA) in various sample types including cell-line biological samples, clinical serum specimens, and nasopharyngeal swab samples. The exhibited simplicity, single-molecule quantitation capability, and broad applicability may render this method a promising candidate for the next generation of RNA diagnostic technology.

Since the ultralocalized Cas13a assay leverages target-activated and cleavage-based signal accumulation to achieve single-molecule detection, the input target RNA itself is subsequently cleaved and degraded after the activation of collateral cleavage,[32] thus eradicating the most frequent contamination risk due to NAA self-replication in conventional molecular laboratories. This means no more specialized infrastructures such as complex air circulation control and strict physical space isolation are required in the case of the ultralocalized Cas13a assay. Moreover, this assay is isothermal and just requires one-step sample loading in the entire workflow, thus avoiding the need for expensive thermocyclers and professional technicians. Additionally, it provides absolute digital quantification and relieves the use of internal reference or calibration. These are desirable features that facilitate the

https://dx.doi.org/10.1021/acsnano.0c08165
ACS Nano XXXX, XXX, XXX−XXX

precise diagnostics being implemented at limited resource settings, particularly during highly infectious disease outbreaks, such as COVID-19.[43,44]

However, some limitations exist in the current version of the ultralocalized Cas13a assay, including multiplexed detection and droplet readout. Further work needs to be done to expand its multiplexing capability and improve the droplet detection, such as employing the orthogonal Cas13a enzymes,[41] using spatially multiplexed chip design,[45] and smartphone-enabled digital detection.[46]

CONCLUSION

In summary, the ultralocalized Cas13a assay represents a simple technology for absolute digital quantitation of single unlabeled RNA molecules, without the need of reverse transcription and sequence amplification. Its excellent sensitivity, specificity, and expandable applicability for precisely counting microRNAs, 16S rRNAs, and SARS-CoV-2 RNA from synthetic sequences to clinical samples are experimentally demonstrated. Thus, we anticipate this technology to be a powerful tool in quantitative molecular biology and clinically precise diagnostics.

MATERIALS AND METHODS

LbuCas13a Protein Expression and Purification. Briefly, *Escherichia coli* Rosetta 2 (DE3) cells harboring pET28a-His6-SUMO-LbuCas13a plasmids, a gift from professor Yanli Wang, were cultured at 37 °C until OD_{600} = 0.6, using Terrific Broth growth media (OXOID) with 100 mg/mL ampicillin (Sangon). Then, 100 μM isopropyl-1-thio-*b*-D-galactopyranoside (IPTG, Sigma) was added to the culture to induce protein expression at 26 °C for 4 h. The cells were harvested and lysed by sonication in lysis buffer (20 mM Tris-HCl, 1 M NaCl, 10% glycerol, pH 7.5). The cell lysate was separated by centrifugation at 8000 rpm at 4 °C, and the collected supernatant was incubated by Ni-NTA agarose (Abiotech, Jinan, China). The bound protein was washed with washing buffer (20 mM Tris-HCl, 150 mM NaCl, 20 mM imidazole, 10% glycerol, pH 7.5) and eluted into an elution buffer (20 mM Tris-HCl, 150 mM NaCl, 500 mM imidazole, 10% glycerol, pH 7.5). Then, the His6-SUMO tags was digested using *Ulp*1 protease. After that, the resulting protein was purified using heparin agarose (Abiotech, Jinan, China). The bound protein was washed using washing buffer (20 mM Tris-HCl, 150 mM NaCl, 10% glycerol, pH 7.5) and eluted into elution buffer (20 mM Tris-HCl, 1 M NaCl, 10% glycerol, pH 7.5). The final protein was dissolved in protein storage buffer (20 mM Tris-HCl, 1 M NaCl, 50% glycerol, pH 7.5) and stored at −80 °C for use (characterization detailed in Supplementary Figure S15).

Preparation of crRNA by *in Vitro* Transcription. DNA templates containing the T7 promoter for *in vitro* crRNA transcription were prepared with the complementary sequence, *via* gradient annealing (95 °C for 5 min followed by cooling to room temperature at a ramp rate of 5 °C/min). The T7 transcription reaction, including DNA templates, T7 RNA polymerase (NEB), and an NTP mix in 1× reaction buffer (40 mM Tris-HCl, 2 mM spermidine, 1 mM DTT, 6 mM $MgCl_2$, pH 7.9), was performed at 37 °C for 4 h. The concentration of crRNA was measured by a Nanodrop 2000 (Thermo Fisher Scientific) and then stored at −80 °C until use.

Cell Culture and Total Small RNA Extraction. Hs578Bst, MDA-MB231, MCF7, and U87 cell lines were grown in Dulbecco's modified Eagle medium (Gibco) and supplemented with 10% FBS (Excell Bio) at 37 °C in a humid atmosphere containing 5% CO_2. Total small RNA was extracted from the cell lines mentioned above using RNAiso for small RNA (Takara) according to the manufacturer's protocol.

Total Small RNA Extraction from Serum Samples. Whole blood samples of healthy volunteers and breast cancer patients were obtained from Central Hospital of Panyu District (Guangdong, China), which were approved by the ethics committee of the hospital in accordance with the Helsinki Declaration. In this study, peripheral blood was derived and separated within 2 h. We introduced synthetic *C. elegans* miR-39, which is absent in the human genome, in order to normalize the efficiency variations in total small RNA extraction. For each serum sample, 1 nM miR-39 was added at a spiked ratio of 1:100 (v/v), and the resulting serum in 200 μL underwent total small RNA extraction using the miRcute serum/plasma miRNA isolation kit (Tiangen) according to the manufacturer's protocol.

Bacterial Strains and RNA Extraction. *Pseudomonas aeruginosa* (ATCC 15442), *Staphylococcus aureus* (ATCC 25923), and *Escherichia coli* (ATCC 35150) were cultured in sterile LB broth (Sangon Biotech, Shanghai, China) overnight at 160 rpm/min at 37 °C. *Enterococcus faecalis* (ATCC 29212) and *Klebsiella pneumoniae* (ATCC 700603) were inoculated on blood plate medium (Antu Bioengineering, Zhengzhou, Henan, China) and cultured at 37 °C for 24 h. All the bacteria strains were harvested at 5000 rpm for 10 min by centrifugation. Total small RNA was extracted from bacteria strains mentioned above using the HiPure bacterial RNA kit (Magen, Guangzhou, China) according to the manufacturer's protocol. The resulting total RNAs were quantified by a Nanodrop 2000 (Thermo Fisher) and stored at −80 °C for later use.

RNA Preparation for SARA-Cov-2 Experiments. SARS-CoV-2 RNA standards was purchased from National Institute of Metrology, China. The standards included three *in vitro* transcriptions (IVT) of key characteristic genes of SARS-CoV-2: the N-gene (full length), the E-gene (full length), and an Orf1ab gene fragment (genomic position: 13201−15600, GeneBank No. NC-045512). The claimed RNA concentrations of the three transcripts were determined by droplet digital PCR.

RNA sequences for the specificity validation were IVT products, which were prepared by the following steps. First, plasmids with a T7 promoter and the whole N-gene sequence of SARS-CoV or bat SARS-like coronavirus inserted were constructed. Then, linear DNA templates of these genes of interest were obtained by PCR amplification of the synthesized plasmids. For PCR reaction, 50 μL of reaction mixture comprised 200 pg of plasmid DNA, 400 nM forward primer (5′-CCTCTAATACGACTCACTATAGGC-3′), 400 nM reverse primer (5′-AACCCCTCAAGACCCGTTTAG-3′), and 1× Prime STAR Max Premix (Takara), and the reaction was performed by Thermal Cycler Dice real time system (Takara). Cycling conditions: 98 °C × 10 s (1 cycle), 30 cycles of 55 °C × 5 s, and 72 °C × 10 s. Afterward, the corresponding RNA transcripts were generated by the T7 transcription reaction. Here, the reaction mixture containing IVT templates, T7 RNA polymerase (NEB), and the NTP mix in 1× RNAPol reaction buffer (40 mM Tris-HCl, 2 mM spermidine, 1 mM DTT, 6 mM $MgCl_2$, pH 7.9) was isothermally incubated at 37 °C for 4 h. The resulting transcripts were purified using the Monarch RNA cleanup kit (NEB) and further quantified by a Nanodrop 2000 (Thermo Fisher Scientific).

Full-length SARS-Cov-2 RNAs were extracted from the cultured SARS-CoV-2 in Huh7.5 cells, which were inactivated before RNA extraction. RNA extraction was implemented by the advanced automatic extraction platform (Qiagen, EZ1), according to the manufacturer's protocol in the P3 biosafety laboratory of Hubei Provincial Center for Disease Control and Prevention.

Nasopharyngeal swab samples were collected from suspected COVID-19 patients in Wuhan, China (during March 2020). The RNA extraction of these swab specimens was also implemented by the automatic extraction platform (Qiagen, EZ1) in the P3 biosafety laboratory of Hubei Provincial Center for Disease Control and Prevention. All procedures complied with the Ethics Committee of Hubei Provincial Center for Disease Control and Prevention/Academy of Preventive Medicine (2020-061-01).

Bulk Fluorescence Detection. Unless otherwise indicated, 25 μL of Cas13a mix was prepared with 20 nM LbuCas13a, 10 nM crRNA, 500 nM FQ5U RNA reporter, a certain amount of target RNA, and 1× reaction buffer (10 mM Tris-HCl, 1.5 mM $MgCl_2$, 50 mM KCl, pH 8.9). The RNA sequences including miRNAs, crRNAs, and RNA reporters are listed in Supplementary Note 3. The bulk

https://dx.doi.org/10.1021/acsnano.0c08165
ACS Nano XXXX, XXX, XXX−XXX

fluorescence detection was performed at 37 °C for 70 min using the Thermal Cycler Dice real time system (Takara), with fluorescence collected every minute.

Real-Time PCR Quantification of MicroRNA. The reverse transcription (RT) cocktail contains 100 nM stem-loop RT primer, dNTP mix (0.5 mM each) (Takara), synthetic miRNA-17 or 100 ng of extracted small RNA, 1 unit/μL RNase inhibitor (NEB), 5 unit/μL SMART MMLV reverse transcriptase (Takara), and 1× MMLV buffer. The RT reaction was carried out at 42 °C for 60 min, then terminated by heating at 70 °C for 15 min. For the real-time PCR reaction, 50 μL of reaction mixture consisting of 2 μL of cDNA, 800 nM forward primer, 400 nM reverse primer, 250 nM Taqman MGB probe, and 1× Probe qPCR Mix (Takara) was used in the Thermal Cycler Dice real time system (Takara). Cycling conditions: 95 °C × 30 s (1 cycle), 40 cycles of 95 °C × 5 s, and 60 °C × 1 min.

Droplet Digital PCR Quantification of MicroRNA. For the ddPCR reaction, 25 μL of reaction mixture comprising 1 μL of cDNA, 800 nM forward primer, 400 nM reverse primer, 250 nM Taqman MGB probe, and 1× ddPCR Supermix for probes (BIO-RAD) was used in the QX200 Droplet Digital PCR system (BIO-RAD). Cycling conditions for the ddPCR reaction are 95 °C × 10 min, 40 cycles of 94 °C × 30 s, and 60 °C × 1 min, then 98 °C for 10 min. After thermal cycling, the droplets were read and analyzed by a QX200 droplet reader (BIO-RAD). The details of the workflow including droplet generation, droplet transfer, and heat sealing were conducted according to the manufacturer's protocol.

Real-Time PCR Experiment of SARS-CoV-2. A CFDA-approved RT-qPCR diagnostic kit (BioGerm from Shanghai BioGerm Medical Biotechnology) was used for detection of SARS-CoV-2 RNA. The 25 μL reaction contains 12 μL of reaction premix, 4 μL of enzyme mixture, 4 μL of Orf1ab/N primer pairs and probe mixture, and 5 μL of RNA samples. The reaction was performed by a Bio-Rad CFX96 Touch. Cycling conditions: 50 °C × 1 min (1 cycle), 95 °C × 5 min (1 cycle), 40 cycles of 95 °C × 10 s, and 55 °C × 40 s. The criteria in this kit were as follows: a Ct value ≤ 38 is positive, a Ct value > 38 is negative.

Microfluidic Chip Design and Fabrication. The mask design for the microfluidic chip is shown in Supplementary Figure S16. The overall architecture of our microfluidic chip simply consists of a single-piece of polydimethylsiloxane (PDMS) irreversibly bonded on a slide glass (Supplementary Figure.S1). The microfluidic chip has one sample inlet for the dispersed phase, a pair of oil inlets for the continuous phase, and an outlet connecting to a syringe. These inlets open to the atmosphere and are maintained at an almost constant pressure (~1 atm); a pressure differential through the chip is created to actuate the fluids when the piston of the connecting syringe is pulled outward and locked in a setting volume. A flow-focusing geometry is adopted for droplet generation, followed by a Christmas tree-shaped distribution channel network. This design facilitates constructing a high-density monolayer droplet array within the fluorescence imaging chamber.

The fabrication of the PDMS channel layer was based on a modified version of an established soft lithography procedure. In brief, microchannel architectures were designed using CAD software and transferred into a high-resolution photomask. SU-8 (3025) master molds with a 30 μm channel depth were produced following the protocol from MicroChem. After wafer fabrication, PDMS was mixed in a 1:8 ratio of curing agent to elastomer and subsequently degassed and poured onto the SU-8-on-Si wafer master. PDMS was cured in a convective oven for 0.5 h at 95 °C. Once cured, the PDMS layer was peeled off and punched to form 3.0-mm-diameter inlets and a 0.7-mm-diameter outlet. To bond PDMS to a slide glass (25 × 75 × 1.2 mm), both surfaces were treated with oxygen plasma in a PDC-MG plasma cleaner for 60 s and bound together. Finally, the microfluidic droplet chip was postbaked in a convective oven at 80 °C for at least 24 h.

Droplet Generation. Prior to droplet generation, the microfluidic chip was filled with an oil phase (mineral oil containing the stabilizing surfactants 3% ABIL EM 90 (Degussa) and 0.1% w/w Triton X-100). Then, a single-use plastic syringe was connected to the out inlets of the chip with a length of Teflon tubing (0.6 mm × 0.9 mm, [i.d. × o.d.]). When the capillary force-driven oil flows reach the sample inlet, a 3 μL aliquot of Cas13a mix that was preconfigured at 4 °C was loaded into the sample inlet with a micropipet, ensuring no air-bubbles were trapped in this inlet. To initiate the droplet generation, the piston of the syringe was pulled outward and locked in place with a one-milliliter volume using a binder clip. After the imaging chamber was filled with the microdroplets, the piston was gently pushed back to its starting position, and then the tubing was cut off. The above processes were operated below 25 °C.

Droplet Imaging. The prepared microdroplets along with the microchip underwent a 60 min isothermal reaction using a heating plate. Subsequently, the microfluidic chip was continuously imaged with an inverted microscope (Olympus, IX-71) to record the bright field and fluorescence images of the microdroplets. A 10× magnification objective lens is capable of imaging 1045 × 1390 μm^2 areas, allowing almost 1200−2400 (with different droplet density) microdroplets to be captured in a picture frame. For a single test, the bright field images were used for accumulating the total number of the microdroplets (at least 20 000 droplets), whereas the corresponding fluorescence images (ISO 1600, 4 s exposure time) were used to discriminate the positive droplets with a signal-to-noise ratio above 3. To determinate the average size of the microdroplets, three randomly chosen areas were imaged with a 40× objective, and over 30 droplets in these microscopic images were measured with cellSens software (Olympus).

Digital Quantification. According to the Poisson distribution, the measured concentration (C) was calculated by

$$C = -\frac{\ln(1 - \mathrm{PPD})}{V}$$

where droplet volume (V) is estimated according to the diameter (D),

$$V = \frac{1}{6}\pi D^3$$

and PPD is the proportion of positive droplets.

ASSOCIATED CONTENT

Supporting Information

The Supporting Information is available free of charge at https://pubs.acs.org/doi/10.1021/acsnano.0c08165.

Supplementary notes and figures (PDF)

High-throughput droplet generation using a microfluidic droplet chip (MP4)

AUTHOR INFORMATION

Corresponding Authors

Bowen Shu − *Department of Laboratory Medicine, Guangzhou First People's Hospital, School of Medicine, South China University of Technology, Guangzhou 510180, China; Clinical Molecular Medicine and Molecular Diagnosis Key Laboratory of Guangdong Province, Guangzhou 510180, China;* orcid.org/0000-0002-9704-2471; Email: eyshubw@scut.edu.cn

Xiaoming Zhou − *School of Life Sciences, South China Normal University, Guangzhou 510631, China;* orcid.org/0000-0001-5597-4804; Email: zhouxm@scnu.edu.cn

Authors

Tian Tian − *School of Life Sciences, South China Normal University, Guangzhou 510631, China*

Yongzhong Jiang − *Key Laboratory of Analytical Chemistry for Biology and Medicine (Ministry of Education), College of Chemistry and Molecular Sciences, Wuhan University,*

https://dx.doi.org/10.1021/acsnano.0c08165
ACS Nano XXXX, XXX, XXX−XXX

Wuhan 430072, China
Miaomiao Ye − *Hubei Provincial Center for Disease Control and Prevention, Wuhan 430079, China*
Lei Liu − *Institute for Brain Research and Rehabilitation, Guangdong Key Laboratory of Mental Health and Cognitive Science, Center for Studies of Psychological Application, South China Normal University, Guangzhou 510631, China*
Zhonghui Guo − *Department of Clinical Laboratory Medicine, Guangzhou 511400, China*
Zeping Han − *Department of Clinical Laboratory Medicine, Guangzhou 511400, China*
Zhang Wang − *Institute of Ecological Science, School of Life Sciences, South China Normal University, Guangzhou 510180, China*

Complete contact information is available at: https://pubs.acs.org/10.1021/acsnano.0c08165

Author Contributions

X.M.Z., T.T., and B.W.S. conceived the concept and designed the study. T.T. and X.M.Z. designed and constructed the Cas13 system. T.T. and L.L. carried out cell culture, total small RNA extraction, bulk fluorescence detection, and all PCR experiments. Y.Z.J., M.M.Y., Z.H.G., and Z.P.H. assisted in clinical sample analysis. W.Z. wrote code for identifying species-specific crRNA sequences. B.W.S. designed and constructed the microfluidic droplet analysis platform for the ultralocalized Cas13a assay. B.W.S. and T.T. performed the ultralocalized Cas13a assay and wrote the manuscript. All authors commented on and edited the manuscript.

Notes

The authors declare no competing financial interest.

ACKNOWLEDGMENTS

We thank Professor Yanli Wang for providing pET28a-His6-SUMO-LbuCas13a plasmids for expressing LbuCas13a. We also thank Zhenguo Zhu for helpful software programing in droplet counting. This work is supported by the National Natural Science Foundation of China (21804044, 21475048, 21874049, and 91959128), Guangzhou Science and Technology Program (201904010413), the Fundamental Research Funds for the Central Universities (2019MS134), and Guangdong Basic and Applied Basic Research Foundation (2020A1515010754).

REFERENCES

(1) Pall, G. S.; Hamilton, A. J. Improved Northern Blot Method for Enhanced Detection of Small RNA. *Nat. Protoc.* **2008**, *3*, 1077−1084.
(2) Tsanov, N.; Samacoits, A.; Chouaib, R.; Traboulsi, A.-M.; Gostan, T.; Weber, C.; Zimmer, C.; Zibara, K.; Walter, T.; Peter, M.; Bertrand, E.; Mueller, F. SmiFISH and FISH-Quant−A Flexible Single RNA Detection Approach with Super-Resolution Capability. *Nucleic Acids Res.* **2016**, *44*, No. e165.
(3) Wang, C.; Gong, B.; Bushel, P. R.; Thierry-Mieg, J.; Thierry-Mieg, D.; Xu, J.; Fang, H.; Hong, H.; Shen, J.; Su, Z.; Meehan, J.; Li, X.; Yang, L.; Li, H.; Łabaj, P. P.; Kreil, D. P.; Megherbi, D.; Gaj, S.; Caiment, F.; Delft, J. V.; et al. The Concordance between RNA-Seq and Microarray Data Depends on Chemical Treatment and Transcript Abundance. *Nat. Biotechnol.* **2014**, *32*, 926−932.
(4) Baker, M. MicroRNA Profiling: Separating Signal from Noise. *Nat. Methods* **2010**, *7*, 687−692.
(5) Eis, P. S.; Olson, M. C.; Takova, T. Y.; Curtis, M. L.; Olson, S. M.; Vener, T. I.; Ip, H. S.; Vedvik, K. L.; Bartholomay, C. T.; Allawi, H. T.; Ma, W.-P.; Hall, J. G.; Morin, M. D.; Rushmore, T. H.; Lyamichev, V. I.; Kwiatkowski, R. W. An Invasive Cleavage Assay for Direct Quantitation of Specific RNAs. *Nat. Biotechnol.* **2001**, *19*, 673−676.
(6) Canady, T. D.; Li, N.; Smith, L. D.; Lu, Y.; Kohli, M.; Smith, A. M.; Cunningham, B. T. Digital-Resolution Detection of MicroRNA with Single-Base Selectivity by Photonic Resonator Absorption Microscopy. *Proc. Natl. Acad. Sci. U. S. A.* **2019**, *116*, 19362−19367.
(7) Geiss, G. K.; Bumgarner, R. E.; Birditt, B.; Dahl, T.; Dowidar, N.; Dunaway, D. L.; Fell, H. P.; Ferree, S.; George, R. D.; Grogan, T.; James, J. J.; Maysuria, M.; Mitton, J. D.; Oliveri, P.; Osborn, J. L.; Peng, T.; Ratcliffe, A. L.; Webster, P. J.; Davidson, E. H.; Hood, L.; et al. Direct Multiplexed Measurement of Gene Expression with Color-Coded Probe Pairs. *Nat. Biotechnol.* **2008**, *26*, 317−325.
(8) Neely, L. A.; Patel, S.; Garver, J.; Gallo, M.; Hackett, M.; McLaughlin, S.; Nadel, M.; Harris, J.; Gullans, S.; Rooke, J. A Single-Molecule Method for the Quantitation of MicroRNA Gene Expression. *Nat. Methods* **2006**, *3*, 41−46.
(9) Husale, S.; Persson, H. H. J.; Sahin, O. DNA Nanomechanics Allows Direct Digital Detection of Complementary DNA and MicroRNA Targets. *Nature* **2009**, *462*, 1075−1078.
(10) Wang, Y.; Zheng, D.; Tan, Q.; Wang, M. X.; Gu, L.-Q. Nanopore-Based Detection of Circulating MicroRNAs in Lung Cancer Patients. *Nat. Nanotechnol.* **2011**, *6*, 668−674.
(11) Johnson-Buck, A.; Su, X.; Giraldez, M. D.; Zhao, M.; Tewari, M.; Walter, N. G. Kinetic Fingerprinting to Identify and Count Single Nucleic Acids. *Nat. Biotechnol.* **2015**, *33*, 730−732.
(12) Cohen, L.; Hartman, M. R.; Amardey-Wellington, A.; Walt, D. R. Digital Direct Detection of MicroRNAs Using Single Molecule Arrays. *Nucleic Acids Res.* **2017**, *45*, No. e137.
(13) Tavallaie, R.; McCarroll, J.; Grand, M. L.; Ariotti, N.; Schuhmann, W.; Bakker, E.; Tilley, R. D.; Hibbert, D. B.; Kavallaris, M.; Gooding, J. J. Nucleic Acid Hybridization on an Electrically Reconfigurable Network of Gold-Coated Magnetic Nanoparticles Enables MicroRNA Detection in Blood. *Nat. Nanotechnol.* **2018**, *13*, 1066−1071.
(14) Chandrasekaran, A. R.; Maclsaac, M.; Dey, P.; Levchenko, O.; Zhou, L.; Andres, M.; Dey, B. K.; Halvorsen, K. Cellular MicroRNA Detection with miRacles: MicroRNA-Activated Conditional Looping of Engineered Switches. *Sci. Adv.* **2019**, *5*, No. eaau9443.
(15) Chen, C.; Ridzon, D. A.; Broomer, A. J.; Zhou, Z.; Lee, D. H.; Nguyen, J. T.; Barbisin, M.; Xu, N. L.; Mahuvakar, V. R.; Andersen, M. R.; Lao, K. Q.; Livak, K. J.; Guegler, K. J. Real-Time Quantification of MicroRNAs by Stem−Loop RT−PCR. *Nucleic Acids Res.* **2005**, *33*, No. e179.
(16) Androvic, P.; Valihrach, L.; Elling, J.; Sjoback, R.; Kubista, M. Two-Tailed RT-qPCR: A Novel Method for Highly Accurate miRNA Quantification. *Nucleic Acids Res.* **2017**, *45*, No. e144.
(17) Yan, L.; Zhou, J.; Zheng, Y.; Gamson, A. S.; Roembke, B. T.; Nakayama, S.; Sintim, H. O. Isothermal Amplified Detection of DNA and RNA. *Mol. BioSyst.* **2014**, *10*, 970−1003.
(18) Chertow, D. S. Next-Generation Diagnostics with CRISPR. *Science* **2018**, *360*, 381−382.
(19) Li, Y.; Li, S.; Wang, J.; Liu, G. CRISPR/Cas Systems towards Next-Generation Biosensing. *Trends Biotechnol.* **2019**, *37*, 730−743.
(20) Shan, Y.; Zhou, X.; Huang, R.; Xing, D. High-Fidelity and Rapid Quantification of miRNA Combining crRNA Programmability and CRISPR/Cas13a Trans -Cleavage Activity. *Anal. Chem.* **2019**, *91*, 5278−5285.
(21) Qin, P.; Park, M.; Alfson, K. J.; Tamhankar, M.; Carrion, R.; Patterson, J. L.; Griffiths, A.; He, Q.; Yildiz, A.; Mathies, R.; Du, K. Rapid and Fully Microfluidic Ebola Virus Detection with CRISPR-Cas13a. *ACS Sensors* **2019**, *4*, 1048−1054.
(22) East-Seletsky, A.; O'connell, M. R.; Knight, S. C.; Burstein, D.; Cate, J. H. D.; Tjian, R.; Doudna, J. A. Two Distinct RNase Activities of CRISPR-C2c2 Enable Guide-RNA Processing and RNA Detection. *Nature* **2016**, *538*, 270−273.
(23) Gootenberg, J. S.; Abudayyeh, O. O.; Lee, J. W.; Essletzbichler, P.; Dy, A. J.; Joung, J.; Verdine, V.; Donghia, N.; Daringer, N. M.; Freije, C. A.; Myhrvold, C.; Bhattacharyya, R. P.; Livny, J.; Regev, A.; Koonin, E. V.; Hung, D. T.; Sabeti, P. C.; Collins, J. J.; Zhang, F.

Nucleic Acid Detection with CRISPR-Cas13a/C2c2. *Science* **2017**, *356*, 438−442.
(24) Kellner, M. J.; Koob, J.; Gootenberg, J. S.; Abudayyeh, O. O.; Zhang, F. SHERLOCK: Nucleic Acid Detection with CRISPR Nucleases. *Nat. Protoc.* **2019**, *14*, 2986−3012.
(25) Kaminski, M. M.; Alcantar, M. A.; Lape, I. T.; Greensmith, R.; Huske, A. C.; Valeri, J. A.; Marty, F. M.; Klämbt, V.; Azzi, J.; Akalin, E.; Riella L, V.; Collins, J. J. A CRISPR-Based Assay for the Detection of Opportunistic Infections Post-Transplantation and for the Monitoring of Transplant Rejection. *Nat. Biomed. Eng.* **2020**, *4*, 601−609.
(26) Patchsung, M.; Jantarug, K.; Pattama, A.; Aphicho, K.; Suraritdechachai, S.; Meesawat, P.; Sappakhaw, K.; Leelahakorn, N.; Ruenkam, T.; Wongsatit, T.; Athipanyasilp, N.; Eiamthong, B.; Lakkanasirorat, B.; Phoodokmai, T.; Niljianskul, N.; Pakotiprapha, D.; Chanarat, S.; Homchan, A.; Tinikul, R.; Kamutira, P.; et al. Clinical Validation of a Cas13-Based Assay for the Detection of SARS-CoV-2 RNA. *Nat. Biomed. Eng.* **2020** DOI: 10.1038/s41551-020-00603-x.
(27) Agapakis, C. M.; Boyle, P. M.; Silver, P. A. Natural Strategies for the Spatial Optimization of Metabolism in Synthetic Biology. *Nat. Chem. Biol.* **2012**, *8*, 527−535.
(28) Ellis, R. J. Macromolecular Crowding: An Important but Neglected Aspect of the Intracellular Environment. *Curr. Opin. Struct. Biol.* **2001**, *11*, 114−119.
(29) Albayrak, C.; Jordi, C. A.; Zechner, C.; Lin, J.; Bichsel, C. A.; Khammash, M.; Tay, S. Digital Quantification of Proteins and mRNA in Single Mammalian Cells. *Mol. Cell* **2016**, *61*, 914−924.
(30) Baker, M. RNA Imaging in Situ. *Nat. Methods* **2012**, *9*, 787−790.
(31) Abudayyeh, O. O.; Gootenberg, J. S.; Konermann, S.; Joung, J.; Slaymaker, I. M.; Cox, D. B.; Shmakov, S.; Makarova, K. S.; Semenova, E.; Minakhin, L.; Severinov, K.; Regev, A.; Lander, E. S.; Koonin, E. V.; Zhang, F. C2c2 Is a Single-Component Programmable RNA-Guided RNA-Targeting CRISPR Effector. *Science* **2016**, *353*, No. aaf5573.
(32) Liu, L.; Li, X.; Ma, J.; Li, Z.; You, L.; Wang, J.; Wang, M.; Zhang, X.; Wang, Y. The Molecular Architecture for RNA-Guided RNA Cleavage by Cas13a. *Cell* **2017**, *170*, 714−726.
(33) Liu, L.; Li, X.; Wang, J.; Wang, M.; Chen, P.; Yin, M.; Li, J.; Sheng, G.; Wang, Y. Two Distant Catalytic Sites Are Responsible for C2c2 RNase Activities. *Cell* **2017**, *168*, 121−134.
(34) Asaga, S.; Kuo, C.; Nguyen, T.; Terpenning, M.; Giuliano, A. E.; Hoon, D. S. Direct Serum Assay for MicroRNA-21 Concentrations in Early and Advanced Breast Cancer. *Clin. Chem.* **2011**, *57*, 84−91.
(35) Barry, T.; Geary, S.; Hannify, S.; MacGearailt, C.; Shalloo, M.; Heery, D.; Gannon, F.; Powell, R. Rapid Mini-Preparations of Total RNA from Bacteria. *Nucleic Acids Res.* **1992**, *20*, 4940.
(36) Elsholz, B.; Wörl, R.; Blohm, L.; Albers, J.; Feucht, H.; Grunwald, T.; Jürgen, B.; Schweder, T.; Hintsche, R. Automated Detection and Quantitation of Bacterial RNA by Using Electrical Microarrays. *Anal. Chem.* **2006**, *78*, 4794−4802.
(37) Broughton, J. P.; Deng, X.; Yu, G.; Fasching, C. L.; Servellita, V.; Singh, J.; Miao, X.; Streithorst, J. A.; Granados, A.; Zorn, K.; Gopez, A.; Hsu, E.; Gu, W.; Miller, S.; Pan, C.-Y.; Guevara, H.; Wadford, D. A.; Chen, J. S.; Chiu, C. Y.; Sotomayor-Gonzalez, A. CRISPR−Cas12-Based Detection of SARS-CoV-2. *Nat. Biotechnol.* **2020**, *38*, 870−874.
(38) Pickar-Oliver, A.; Gersbach, C. A. The Next Generation of CRISPR−Cas Technologies and Applications. *Nat. Rev. Mol. Cell Biol.* **2019**, *20*, 490−507.
(39) Sander, J. D.; Joung, J. K. CRISPR-Cas Systems for Editing, Regulating and Targeting Genomes. *Nat. Biotechnol.* **2014**, *32*, 347−355.
(40) Bruch, R.; Baaske, J.; Chatelle, C.; Meirich, M.; Madlener, S.; Weber, W.; Dincer, C.; Urban, G. A. CRISPR/Cas13a-Powered Electrochemical Microfluidic Biosensor for Nucleic Acid Amplification-Free miRNA Diagnostics. *Adv. Mater.* **2019**, *31*, 1905311.
(41) Gootenberg, J. S.; Abudayyeh, O. O.; Kellner, M. J.; Joung, J.; Collins, J. J.; Zhang, F. Multiplexed and Portable Nucleic Acid Detection Platform with Cas13, Cas12a, and Csm6. *Science* **2018**, *360*, 439−444.
(42) Bartel, D. P. MicroRNAs: Genomics, Biogenesis, Mechanism, and Function. *Cell* **2004**, *116*, 281−297.
(43) Udugama, B.; Kadhiresan, P.; Kozlowski, H. N.; Malekjahani, A.; Osborne, M.; Li, V. Y.; Chen, H.; Mubareka, S.; Gubbay, J. B.; Chan, W. C. W. Diagnosing COVID-19: the Disease and Tools for Detection. *ACS Nano* **2020**, *14*, 3822−3835.
(44) Huang, H.; Fan, C.; Li, M.; Nie, H.-L.; Wang, F.-B.; Wang, H.; Wang, R.; Xia, J.; Zheng, X.; Zuo, X.; Huang, J. COVID-19: A Call for Physical Scientists and Engineers. *ACS Nano* **2020**, *14*, 3747−3754.
(45) Yin, J.; Zou, Z.; Yin, F.; Liang, H.; Hu, Z.; Fang, W.; Lv, S.; Zhang, T.; Wang, B.; Mu, Y. A Self-Priming Digital Polymerase Chain Reaction Chip for Multiplex Genetic Analysis. *ACS Nano* **2020**, *14* (8), 10385−10393.
(46) Yelleswarapu, V.; Buser, J. R.; Haber, M.; Baron, J.; Inapuri, E.; Issadore, D. Mobile Platform for Rapid Sub−Picogram-Per-Milliliter, Multiplexed, Digital Droplet Detection of Proteins. *Proc. Natl. Acad. Sci. U. S. A.* **2019**, *116* (10), 4489−4495.

https://dx.doi.org/10.1021/acsnano.0c08165
ACS Nano XXXX, XXX, XXX−XXX